The ascending median raphe projections are mainly glutamatergic in the mouse forebrain

András Szőnyi,
Laboratory of Cerebral Cortex Research, Institute of Experimental Medicine Hungarian Academy of Sciences, Budapest 1083, Hungary, János Szentágothai Doctoral School of Neurosciences, Semmelweis University, Budapest 1085, Hungary

Márton I. Mayer,
Laboratory of Cerebral Cortex Research, Institute of Experimental Medicine Hungarian Academy of Sciences, Budapest 1083, Hungary

Csaba Cserép,
Laboratory of Cerebral Cortex Research, Institute of Experimental Medicine Hungarian Academy of Sciences, Budapest 1083, Hungary

Virág T. Takács,
Laboratory of Cerebral Cortex Research, Institute of Experimental Medicine Hungarian Academy of Sciences, Budapest 1083, Hungary

Masahiko Watanabe,
Department of Anatomy, Hokkaido University School of Medicine, Sapporo 060-8638, Japan

Tamás F. Freund, and
Laboratory of Cerebral Cortex Research, Institute of Experimental Medicine Hungarian Academy of Sciences, Budapest 1083, Hungary

Gábor Nyiri
Laboratory of Cerebral Cortex Research, Institute of Experimental Medicine Hungarian Academy of Sciences, Budapest 1083, Hungary

Gábor Nyiri: nyiri.gabor@koki.mta.hu

Abstract

The median raphe region (MRR) is thought to be serotonergic and plays an important role in the regulation of many cognitive functions. In the hippocampus (HIPP), the MRR exerts a fast excitatory control, partially through glutamatergic transmission, on a subpopulation of GABAergic interneurons that are key regulators of local network activity. However, not all receptors of this connection in the HIPP and in synapses established by MRR in other brain areas are known. Using combined anterograde tracing and immunogold methods, we show that the GluN2A subunit of the NMDA receptor is present in the synapses established by MRR not only in the HIPP, but also in the medial septum (MS) and in the medial prefrontal cortex (mPFC) of the mouse. We estimated similar amounts of NMDA receptors in these synapses established by the

Correspondence to: Gábor Nyiri, nyiri.gabor@koki.mta.hu.

MRR and in local adjacent excitatory synapses. Using retrograde tracing and confocal laser scanning microscopy, we found that the majority of the projecting cells of the mouse MRR contain the vesicular glutamate transporter type 3 (vGluT3). Furthermore, using double retrograde tracing, we found that single cells of the MRR can innervate the HIPP and mPFC or the MS and mPFC simultaneously, and these double-projecting cells are also predominantly vGluT3-positive. Our results indicate that the majority of the output of the MRR is glutamatergic and acts through NMDA receptor-containing synapses. This suggests that key forebrain areas receive precisely targeted excitatory input from the MRR, which is able to synchronously modify activity in those regions via individual MRR cells with dual projections.

Keywords

Median raphe; NMDA receptor; Vesicular glutamate transporter type 3; vGluT3; GABAergic interneurons; Immunohistochemistry; Non-serotonergic; Hippocampus; Medial septum; Prefrontal cortex; Mouse

Introduction

The midbrain raphe nuclei are responsible for the serotonergic innervation of the forebrain (Azmitia and Segal 1978; Vertes and Martin 1988). The dorsal raphe (DR) and median raphe region (MRR) are thought to play a very important role in modulating different brain functions like emotions, mood, learning and memory (Vertes and Kocsis 1997; Hensler 2006). Although they are both serotonergic, DR and MRR show a very different pattern of innervation in the forebrain. While DR sends thin fibers establishing hardly any synaptic contacts, the thick fibers of the MRR typically influence its targets via synaptic connections (Kosofsky and Molliver 1987; Leranth and Vertes 1999; Varga et al. 2009; Bang et al. 2012). The MRR that corresponds to the median raphe (MR) and paramedian raphe (PMR) subregions, strongly innervates many cortical and subcortical forebrain areas, including the hippocampus (HIPP), medial septum (MS) and medial prefrontal cortex (mPFC; Vertes et al. 1999; Bang et al. 2012). Although the exact targets of MRR are not known in every innervated brain area, MRR projection seems to be very specific in the HIPP and MS. In the HIPP of the rat, MRR establishes synaptic contacts with the somata or proximal dendrites of different types of interneurons, except parvalbumin-positive cells (Freund et al. 1990; Acsády et al. 1993; Papp et al. 1999; Somogyi et al. 2004; Varga et al. 2009), and MRR provides a complex modulation of the hippocampal network activity (Assaf and Miller 1978; Vertes and Kocsis 1997; Jackson et al. 2008). In the MS and diagonal band of Broca of the rat, MRR fibers give perisomatic and per-idendritic baskets onto parvalbumin and calbindin-positive GABAergic cells, specifically (Leranth and Vertes 1999; Aznar et al. 2004). These cells are in key position to modulate synchronous network activity in the forebrain (Freund and Antal 1988; Klausberger 2009).

However, projection fibers of the MRR are not only serotonergic (Köhler et al. 1982; Köhler and Steinbusch 1982; Aznar et al. 2004). Some of the cells in the MRR that project to the forebrain also contain vesicular glutamate transporter type 3 (vGluT3) and are considered to be glutamatergic (Varga etal. 2009), although these cells may or may not be 5HT-positive

(Aznar et al. 2004; Jackson et al. 2009). The exact ratios of these cell types are still not known.

Using in vivo and in vitro optogenetical stimulation, previously, we described in the rat that MRR can exert a very fast control of a subpopulation of interneurons in the HIPP, through both serotonergic and glutamatergic neurotransmission (Varga et al. 2009). Whether such a strong glutamatergic control can be mediated also by NMDA-type glutamate receptors or whether NMDA receptor-containing synapses are established by MRR in other target brain areas is unknown. NMDA receptors are key mediators of glutamatergic transmission, playing an important role in synaptic plasticity mechanisms in classical excitatory synapses (Dingledine et al. 1999; Malenka and Bear 2004). NMDARs have heterotetrameric structure with two GluN1 subunits and usually with two GluN2 subunits. GluN2 subunits are not transported to the membrane without forming functional channels with the GluN1 subunits (Fukaya et al. 2003). If NMDA receptors were present in the forebrain synapses of the MRR, these connections would not only be ideal for fast and precise activation or even synchronous modulation of the target areas, but also would account for some of the interactions between glutamatergic and serotonergic modulation described in many different systems (Maura et al. 2000; MacLean and Schmidt 2001; Yuen et al. 2005).

Single serotonergic cells of the rat MRR can project to more than one forebrain areas (Köhler and Steinbusch 1982; Acsády et al. 1996). Although non-serotonergic cells were also shown in these studies to innervate more brain areas simultaneously, the neurochemical identity of these cells was not examined. Therefore, it is still unknown, whether a single glutamatergic cell of the MRR can project to more forebrain areas simultaneously.

vGluT3-positive neurons are not necessarily glutamatergic in all brain areas; for instance, vGluT3-positive interneurons are considered to be only GABAegic in the HIPP (Somogyi et al. 2004). To the best of our knowledge, no studies confirmed so far that these MRR neurons do act via glutamate receptors in the mouse and only one of our previous studies gave evidence that they are indeed glutamatergic in the hippocampus of rat (Varga et al. 2009). Although previously several studies focused on the rat brain, with the advent of genetic engineering, mouse became the model animal for most physiological and anatomical studies, and therefore focusing on this species makes current and future data more interpretable.

Using anterograde tracing combined with double-labeling immunoelectron microscopy in the mouse, here we show that the GluN2A subunit of the NMDA receptors can be present in the postsynaptic active zone of the synapses established by the MRR not only in the HIPP, but also in the MS and in the mPFC. We semiquantitatively estimated that on the average, there is a similar amount of NMDA receptors in the synapses established by the MRR compared to that in the local asymmetric (putative excitatory) synapses.

These glutamatergic synapses may be a key component of the output of MRR, because in retrograde tracing experiments combined with immunofluorescent staining, we found that the majority of the MRR cells projecting to the HIPP, MS and mPFC are in fact glutamatergic. Moreover, confocal laser scanning microscopic analysis of double retrograde tracing experiments revealed that glutamatergic MRR neurons project to more than one

forebrain areas. Our results suggest that projections from the MRR are predominantly glutamatergic, because most cells of the MRR projecting to the HIPP, MS and mPFC contain vGluT3, and in addition, projecting cells can act through synapses containing NMDA receptors. Furthermore, these cells with bifurcating glutamatergic fibers are optimal to synchronously excite inhibitory neurons of different fore-brain areas in a fast and precise manner, which makes the MRR an ideal and fast glutamatergic modulator of its forebrain targets.

Materials and methods

Animals and perfusion

All experiments were performed in accordance with the Institutional Ethical Codex and the Hungarian Act of Animal Care and Experimentation guidelines, which are in concert with the European Communities Council Directive of September 22, 2010 (2010/63/EU). The Animal Care and Experimentation Committee of the Institute of Experimental Medicine of Hungarian Academy of Sciences and the Animal Health and Food Control Station, Budapest, have also approved the experiments.

Fifteen 29–118 days old male C57BL/6 J wild-type mice, and a 174 days old vGluT3$^{-/-}$ null-mutant mouse were sacrificed. For perfusion, mice were anesthetized with isoflurane followed by an intraperitoneal injection of an anesthetic mixture (containing 8.3 mg/ml ketamine, 1.7 mg/ml xylazine-hydrochloride, 0.8 mg/ml promethazinium-chloride) to achieve deep anesthesia. After that the mice were perfused transcardially first with 0.9 % NaCl solution for 2 min followed by 4 % paraformaldehyde for 40 min and finally with 0.1 M phosphate buffer (PB) for 10 min.

Stereotaxic surgery

Ten 49–118 days old male C57BL/6 J wild-type mice were anesthetized with isoflurane followed by an intraperitoneal injection of an anesthetic mixture (containing 8.3 mg/ml ketamine, 1.7 mg/ml xylazine-hydrochloride in 0.9 % saline, 10 ml/kg body weight) and then were mounted in a stereotaxic frame. For anterograde tracing experiments, we injected 5–9 nl 5 % solution of the anterograde tracer biotinylated dextran amine (Lanciego and Wouterlood 2011, BDA; molecular weight 10 kDa; Molecular Probes) into the MRR of three mice. The coordinates for the injection were 4.4 mm posterior from the bregma, in the midline, and 4.5 mm below the level of the horizontal plane defined by the bregma and the lambda (zero level). For the injections, we used a Recording Nanoject-R precision microinjector pump (Drummond, Broomall, PA). We used borosilicate micropipettes (Drummond, Broomall, PA) for the injections with tips broken to 28–36 μm. We tested, if the 10 kDa BDA could travel retrogradely as well in the injected brains, but we found only a very few retrogradely labelled cells in the close vicinity of the MRR, which are highly unlikely to have any fibers in the examined areas. For double retrograde tracing experiments, first, we injected the retrograde tracer 2 % Fluoro-Gold (FG; Fluorochrome, Denver, CO, USA) into the mPFC of seven mice. In three out of the seven mice, FG was injected only into the left hemisphere at the coordinates of 1.8 mm anterior from the bregma, 0.3 mm lateral from the midline and 2.7 mm below the zero level. In these cases, following

FG injections, we injected the retrograde tracer 0.5 % Cholera toxin B subunit (CTB, List Biologicals, Campbell, CA, USA) into the HIPP of the left hemisphere at three coordinates: 2.5, 2.8, 3.2 mm posterior from bregma, 1.6, 1.6, 1.7 mm lateral from midline and 2.1, 2.1, 2.2 mm below the zero level, respectively. In the other four mice, FG was injected bilaterally into the PFC at the coordinates given above, and CTB was injected into the MS at the coordinates 1.0 mm anterior from bregma, in the midline and 4.1 mm below the zero level. We injected 14–18 nl of FG and 18–23 nl of CTB into every single injection spot using the Nanoject-R pump. The coordinates were defined according to the atlas by Paxinos and Franklin (2012). In some cases we used unilateral injections, the reason of which is that the chance of missing the target brain area increases with the number of injections and having more than four injections decreased the chance of the animal to survive. Therefore, we did not want to raise the number of injections in the mPFC-HIPP injected animals, where we already carried out four injections per mouse. After the surgeries, the animals received 0.5–0.7 ml saline and 0.03–0.05 mg/kg meloxicam (Metacam, Boehringer In-gelheim, Germany) intraperitoneally, and we placed them into separate cages to survive for 8–14 days before perfusions.

Antibodies

We summarized the antibodies used in Table 1. The specificity of the antibodies for vesicular glutamate transporter type 3 (vGluT3), neuroligin 2 (NLGN2) and NMDA receptor GluN2A-subunit (GluN2A) was tested extensively before in experiments using wild-type and vGluT3$^{-/-}$, NLGN2$^{-/-}$ or GluN2A$^{-/-}$ null-mutant mice, respectively (Watanabe et al. 1998; Szabadits et al. 2011; Takács et al. 2013). Here, we confirm again the specificity of the guinea pig anti-vGluT3 antibody, using vGluT3$^{-/-}$ null-mutant mice. After subsequent washes in PB and TBS, the sections containing the MRR or HIPP were incubated in a primary antibody solution containing the guinea pig anti-vGluT3 antibody (1:1,000 or 1:4,000, respectively) for 48 h. After subsequent washes in TBS, the sections containing the MRR were incubated in a secondary antibody solution containing Alexa 488 conjugated goat anti-guinea pig antibody (1:1,000), and the sections containing HIPP were incubated in a secondary antibody solution containing biotinylated goat anti-guinea pig antibody (Vector Laboratories, 1:200) overnight. The following treatment and immunoperoxidase reaction were performed as described below. We did not see any specific-like labeling in the vGluT3$^{-/-}$ mouse strain (Fig. 4d$_1$–d$_6$). The anti-FG and anti-CTB antibodies showed no labeling in animals that were not injected with the respective retrograde tracers. The rat anti-serotonin (5HT) antibody was characterized before by (Amilhon et al. 2010) and we also detected a similar staining pattern for serotonin, which further confirms its specificity.

Secondary antibodies were also extensively tested for possible cross-reactivity with the other secondary or primary antibodies used here, and possible tissue labeling without primary antibodies was also tested to exclude autofluorescence or specific background labeling by the secondary antibodies. No specific-like staining was observed under these control conditions.

Double-labeling immunoelectron microscopy

For NLGN2, GluN2A and vGluT3 immunolabeling, after perfusion of four wild-type mice and removal of their brains from the skull, coronal sections were cut on a Leica VT1200S vibratome at 50 μm. This was followed by washing out the fixative in 0.1 M phosphate buffer (PB) for 1 h. Then, the sections were cryo-protected sequentially in 10 % (overnight) and 30 % (2 h) sucrose in PB and freeze-thawed three times over liquid nitrogen. For synaptic detection of NLGN2, the sections were washed subsequently in 0.1 M PB following tris buffered saline (TBS) and blocked in 1 % human serum albumin (HSA; Sigma-Aldrich) in TBS. Then, they were incubated in a mixture of primary antibodies for NLGN2 (rabbit, 1:600) and vGluT3 (guinea pig, 1:3,000) diluted in TBS. For synaptic detection of NMDA receptors, pretreatment with pepsin was essential (Watanabe et al. 1998). The sections were incubated in 0.2 M HCl solution containing 1 mg/ml pepsin (Dako) at 37C° for 10 min. They were then incubated in 50 mM glycine (Sigma-Aldrich) and blocked in 1 % HSA in TBS, followed by incubation in a mixture of primary antibodies for GluN2A subunit (rabbit; 1:250) and vGluT3 (guinea pig; 1:4,000) diluted in TBS containing 0.1 % BSA-c (BSA-c/TBS; Aurion) for 72 h. For anterograde tracing experiments, the primary antibody solution contained only the anti-GluN2A-antibody. After repeated washes in TBS, the sections labeled for NLGN2 were incubated in blocking solution (Gel-BS) containing 0.2 % cold water fish skin gelatine and 0.5 % HSA in TBS for 1 h. The sections labeled for GluN2A were washed intensively in BSA-c/TBS. After this, both series of the sections were incubated in mixtures of secondary antibody solutions containing 1.4 nm gold-conjugated goat anti-rabbit (Fab'-fragment; in a concentration of 1:100 in NLGN2 experiments and 1:300 for GluN2A staining) and biotinylated goat anti-guinea pig (Vector Laboratories, 1:200) diluted in Gel-BS or BSA-c/TBS, respectively, for 24 h. For anterograde tracing experiments, the secondary antibody solution contained only the gold-conjugated goat anti-rabbit antibody. After intensive washes in TBS or BSA-c/TBS, the sections were treated with 2 % glutaraldehyde in 0.1 M PB for 15 min to fix the gold particles into the tissue. To develop the tracer or vGluT3 labeling, this was followed by incubation in avidin–biotinylated horseradish peroxidase complex (Elite ABC; 1:300; Vector Laboratories) diluted in TBS for 3 h. The immunoperoxidase reaction was developed using DAB (3,3-diaminobenzidine; Sigma-Aldrich) as chromogen. To enlarge immunogold particles, this was followed by incubation in silver enhancement solution (SE-EM; Aurion) for 40 min at room temperature. The sections were treated with 0.5 % osmium tetroxide in 0.1 M PB on ice and they were dehydrated in ascending alcohol series and in acetonitrile and embedded in Durcupan (ACM; Fluka). During dehydration, the sections were treated with 1 % uranylacetate in 70 % ethanol for 20 min. After this, the 100-nm-thick serial sections were prepared using an ultramicrotome (Leica EM UC6) and picked up on single-slot copper grids. The sections were examined using a Hitachi H-7100 electron microscope and a Veleta CCD camera.

Analysis of immunogold electron microscopic experiments

Randomly sampled vGluT3-positive terminals establishing synaptic contacts with the somata or proximal dendrites of interneurons located at the border of stratum radiatum and lacunosum-moleculare were fully reconstructed in the HIPP. In tracing experiments, BDA-labeled terminals were randomly sampled and fully reconstructed in the HIPP, MS and

mPFC. The membrane-associated gold particles, i.e. those that were within 40 nm from the membrane, labeling the GluN2A subunit of the NMDA receptors were counted on the postsynaptic side of the synapses established by these terminals to determine the density of gold particles, and the proportion of GluN2A-positive synapses. The reason for using 40 nm is the following. The C-terminus epitope of the NMDAR is located a few nanometers away from the membrane, intracellularly. This is labeled with one antibody, the latter of which is also labeled with yet another antibody. Based on the data obtained with atomic force microscopy and individual-particle electron tomography studies (San Paulo and García 2000; Zhang and Ren 2012), we calculated with 15–18 nm/IgG plus 6–7 nm/Fab'-fragment. These, together with the 10–15 nm diameters of the silver-enhanced gold particles make up the 40-nm band, in which we counted gold particles, to make sure that we do not exclude real labeling.

Gold particles were also counted on the postsynaptic side of fully reconstructed DAB-negative asymmetric (putative glutamatergic excitatory) synapses, on a 200-nm-long extrasynaptic membrane segment measured from both edges of the very same synapses, and to determine the background labeling, we also examined the presynaptic terminal membrane of these synapses. The density of the immunogold particles on the postsynaptic active zones were always 30–120 times higher compared to the background that confirms the specificity of the labeling procedure. We measured the areas of fully reconstructed synapses established by the MRR and by local excitatory terminals in the very same BDA-GluN2A double reactions, in different serial sections. To prevent sampling bias, stereological rules were applied in the experiments. Larger synapses would be sampled more likely, if stereological rules are not observed. To avoid this sampling bias, we randomly sampled synapses in a given tissue volume that started in that volume regardless of the size of the given synapse. Therefore, during reconstruction of asymmetric synapses, we randomly selected synapses that were not present in the lookup section above, but once we selected a synapse, we reconstructed it regardless of its size. The largest asymmetric synapses can be reconstructed from up to six serial sections. Therefore, we used only those tissue volumes, where we could test another six sections below the test volume.

Retrograde tracing and fluorescent confocal microscopy

The stereotaxic injection of the retrograde tracers, perfusion, and sectioning of the brains was performed as described above. In case of four mice, after subsequent washes in PB and TBS, the sections were incubated in a mixture of primary antibodies for FG (rabbit; previously exhausted on native slices in 1:1,000 for 1 h and after that diluted to 1:10,000) and CTB (goat; 1:20,000) for 48–72 h. In case of another three mice, the primary antibody solution contained anti-FG (rabbit; exhausted, 1:10,000), anti-CTB (mouse; 1:400), anti-vGluT3 (guinea pig; 1:1,000) and anti-serotonin (rat; 1:500) antibodies diluted in TBS. After subsequent washes in TBS, the sections were incubated overnight in a mixture of the following secondary antibodies: Alexa 488 conjugated donkey anti-rabbit (1:500) and Alexa 594 conjugated donkey anti-goat (1:500); or Alexa 488 conjugated donkey anti-rabbit (1:500), DyLight 549 conjugated donkey anti-mouse, Alexa 647 conjugated chicken anti-rat (1:500) and biotinylated goat anti-guinea pig (1:200). After that, the second set of vials was washed in TBS for 1 h and incubated in a tertiary solution containing DyLight 405

streptavidin dissolved in TBS for 5 h. After washes in TBS and PB, the sections were transferred to slides, and covered with Aquamount (BDH Chemicals Ltd.).

Analysis of retrograde tracing experiments

Every single injection site was reconstructed from the 50-μm-thick sections using a Zeiss Axioplan2 microscope, to estimate what percentage of the examined brain area was injection labeled with the tracer. Every part of the target tissue containing low levels of the tracer was considered to be the part of the injection site. We fitted every image of the injection sites to the corresponding outlines of the atlas (Paxinos and Franklin 2012), and determined the ratio of the volumes of the injection sites to the examined brain area, using the Fiji/ImageJ software. The brain areas we measured were the following based on the atlas: in case of the hippocampus, the dentate gyrus and the regions CA1-3; in case of the medial septum, the medial septal area and the diagonal bands of Broca; in case of the medial prefrontal cortex, the areas A24a-b (anterior cingulate cortex), A25 (infralimbic cortex), A32 (prelimbic cortex) and medial orbital cortex.

In case of the double-labeling experiments, the 50-μm-thick sections of the midbrain containing the median raphe were analyzed using an Olympus Optical FluoView 300 confocal laser scanning microscope in sequential scanning mode. Every single section of the median raphe region was reconstructed in z-stacks with 5 μm resolution. Cells were counted using Adobe Photoshop software.

In case of the quadruple labeling experiments, we used a Nikon A1R confocal laser scanning microscope system to completely reconstruct every single section in z-stacks with 2 μm resolution. FG or CTB-labeled cells were counted, and their 5HT or vGluT3-content was determined using the NIS Elements software. To prevent stereological bias in these experiments, the relative ratios of the different cell types in these areas were corrected by the size of the cells using Abercrombie's correction.

In every experiment, we analyzed the median raphe (MR) and paramedian raphe (PMR) subregions of the median raphe region (MRR) separately. In every analyzed section, we defined the border of the MRR and its subregions using the atlas (Paxinos and Franklin 2012). During the different measurements, we found no difference between any measured features of the cells located at the two subregions, except that the density of the cells was obviously higher in MR.

Results

NMDA receptors are present in synapses established by MRR in the hippocampus

To examine whether these MRR synapses resemble the classical excitatory synapses, here, we examined whether they contain GluN2A subunit of the NMDA-type glutamate receptors. In the first set of experiments, we injected the anterograde tracer 10 kDa BDA into the MRR of three mice (Fig. 1a), and after 7–10 days of survival, we performed double immunogold–immunoperoxidase labeling for the GluN2A subunit of the NMDA receptors and for BDA. At the light microscopic level, BDA labeling showed the known pattern of MRR innervation in the HIPP (Freund et al. 1990; Vertes et al. 1999), i.e., there were several

immunoperoxidase-positive fibers and terminals in the distal dendritic regions of the hippocampal pyramidal cells, in the outer third of the stratum radiatum and in stratum lacunosum-moleculare. Using correlated light and electron microscopy, we fully reconstructed 42 randomly sampled raphe-hippocampal synapses in the CA1 region of the HIPP, at the distal dendritic regions of hippocampal pyramidal cells ($n = 15$, 12 and 15 in 3 mice, respectively). These synapses target the somata of local inter-neurons or with putative interneuronal dendritic segments. According to our measurements, about one-third of the raphe-hippocampal synapses contained the GluN2A sub-unit in their postsynaptic active zones (Fig. $1b_1$–b_3). For statistical details see Fig. 3c.

We also analyzed the density of immunogold labeling along different membrane segments. Although these preembedding immunogold measurements are only semi-quantitative, they are proved to be suitable for a good approximation of the differences between membrane receptor densities. GluN2A subunit immunogold labeling was present in the postsynaptic active zones of synapses established by MRR terminals and in classical excitatory synapses as well. The density of the immunogold particles in the raphe-hippocampal synapses was not much lower than that in adjacent local classical excitatory synapses. Rarely, immunogold particles were also found in extrasynaptic membrane segments as described previously (Szabadits et al. 2011). The background labeling measured on the presynaptic terminals of classical excitatory synapses was negligible. For statistical details see Fig. 3d.

To estimate the absolute NMDA receptor content of the different kinds of synapses, we measured their synaptic area using fully reconstructed synapses. Our data show that the synapses established by MRR in the HIPP have a larger area than the classical excitatory synapses (Fig. 3e). To calculate the total amount of gold labeling in our synapses, we multiplied the GluN2A immunogold density with the measured areas. We found that the synapses established by MRR and classical excitatory terminals (0.41 ± 0.24 vs. 0.38 ± 0.20 gold particles/synapse, respectively) contain similar amount of average labeling, suggesting that, on average, they act through similar amount of NMDA receptors.

To further confirm these results, we performed another set of experiments using vGluT3-GluN2A double immunolabeling. There are two sources of vGluT3-containing terminals in the HIPP: the first originates from basket cells and establishes synaptic contacts in the stratum pyramidale on the perisomatic region of pyramidal cells, while the second originates from MRR and establishes synapses on the somata and proximal dendrites of interneurons located in the outer third of the stratum radiatum and in stratum lacunosum-moleculare (Somogyi et al. 2004). At the light microscopic level, we found the classical pattern of vGluT3-positive terminal labeling (and we found several immunopositive interneurons as well). Because vGluT3 labels the majority of the terminals of the MRR that innervate the HIPP, we could collect a larger sample of synapses from the surface of the sections, where the immunoreaction was the strongest. Only those synapses were included in these measurements that were established on the somata of interneurons. We found in two mice that almost all of these synapses established by vGluT3-positive terminals ($n = 20$ synapse/mouse) contain the GluN2A subunit of the NMDA receptors (about 90 %, Fig. 1c–e). For exact percentages see Fig. 3a. We also compared the density of the gold particles in the synapses established by vGluT3-positive terminals to that of the adjacent local classical

excitatory synapses, and we found that their ratios are similar to those measured in the anterograde tracing experiments (compare Fig. 3b, d).

However, some terminals of the vGluT3-positive GAB-Aergic basket cells may target the distal dendritic regions. To determine the exact distribution of these basket cell terminals in the distal dendritic layers, we performed double immunogold–immunoperoxidase labeling for neuroligin 2 (NLGN2) and vGluT3. NLGN2 is a postsynaptic transmembrane protein present in the GABAergic (Varoqueaux et al. 2004) and cholinergic synapses (Takács et al. 2013). At the electron microscopic level, NLGN2 labeling was associated with postsynaptic membranes. We found that only about 10 % of the examined vGluT3-positive terminals contained NLGN2 postsynaptically in the CA1 region (49 and 39 serially reconstructed synapses in two mice, respectively; for details, see Fig. 3a). In contrast, adjacent vGluT3-negative (putative GABAergic) symmetric synapses were always NLGN2-positive (Fig. 1f). Taking into account that about 90 % of the synapses established by vGluT3-positive terminals are established by MRR in these layers, at least about 88 % of the MRR-HIPP synapses express NMDA receptors according to these measurements. These data show higher percentages than those found in the tracing experiments, because here we could collect synapses from the surface of sections, where digestion and penetration parameters were more optimal.

NMDA receptors are present in the synapses established by MRR in the MS and mPFC

MRR innervates not only the HIPP, but also many other forebrain areas (Vertes et al. 1999; Bang et al. 2012). To investigate whether NMDA receptors are present in other forebrain areas, we also analyzed BDA-labeled terminals in the MS and in the mPFC. At the light microscopic level, MS shows strong innervation from the MRR. In the mPFC, we found a few basket-like varicosities with approximately 5–10 terminals in a group. Using correlated light and electron microscopy, we fully reconstructed 45 and 44 synapses in the MS (Fig. $2a_1$–a_4, b, c) and in the mPFC (Fig. $2d_1$–d_2, e_1–e_3, f), respectively ($n = 15, 15, 15$ from MS and $n = 15, 14, 15$ for mPFC in three mice, respectively). According to our measurements, at least about 40 % of the synapses established by BDA-positive terminals in the MS and at least about the half of them in the mPFC contained GluN2A in their postsynaptic active zone, respectively (Figs. 2, 3c).

The density of the GluN2A immunogold particles was also measured in the MRR-MS and MRR-mPFC synapses, and these values were not much lower than the immunogold content of adjacent local classical excitatory synapses; for details, see Fig. 3f, h. We found some extrasynaptic membrane immunogold labeling in these areas as well, and only a negligible background labeling.

To estimate the absolute receptor content of the synapses established by MRR in the MS and mPFC, we measured their area, similar to that in the HIPP (see above). We found that on average, the area of the synapses established by MRR in the MS and mPFC is again larger compared to that of the local classical excitatory synapses (Fig. 3g, i). The total amount of gold particles in the MRR-MS and MRR-mPFC synapses was similar to that in the local classical excitatory synapses (0.89 ± 0.48 vs. 0.65 ± 0.40 gold particles/synapse in the MS, and 0.92 ± 0.42 vs. 0.52 ± 0.24 gold particles/synapse in the mPFC, respectively). Taken

together, these data show that the immunolabeling profile is very similar in the three examined target areas (Fig. 3d–i).

The majority of the MRR cells projecting to the forebrain are glutamatergic

Although anterograde tracing experiments showed the abundance of glutamate receptors in synapses established by MRR in the forebrain, we wanted to know whether the presence of vGluT3 is also typical in these projections. We injected the retrograde tracers CTB into the HIPP or MS and FG into the mPFC, and we performed quadruple staining for FG, CTB, vGluT3 and 5HT (Figs. 4, 5). We analyzed the median raphe (MR) and paramedian raphe (PMR) subregions of the median raphe region (MRR) separately, but we found no difference between any measured cell ratios, except that the density of the cells was obviously higher in MR; therefore, we report data pooled for the whole MRR.

Glutamatergic HIPP and MS projections were reported previously in the rat (Jackson et al. 2009) and, here, we confirmed that this is similar in the mouse. In case of the cells projecting to the HIPP, we found that about 80 % of them contain vGluT3 with or without containing 5HT and only 8 % was only 5HT-positive. In case of the cells projecting to the MS, we found that about half of them contain vGluT3 with or without containing 5HT and only about 11.5 % was only 5HT-positive. For exact percentages, see Table 2.

The neurochemical identity of the MRR cells projecting to the mPFC was not examined before. We found that about 70 % of them contain vGluT3, while most of those are only vGluT3-positive and only about 16 % was only 5HT-positive. See Table 2 for details.

Single cells of the MRR project to the HIPP and mPFC simultaneously

If single glutamatergic MRR cells could innervate more than one brain area, they could conduct a highly effective synchronous modulation of the network activity in those forebrain areas; therefore we investigated whether the same MRR cells can project to HIPP and mPFC as well. We injected the retrograde tracers CTB into the HIPP, and FG into the mPFC of the left hemisphere of three mice. Then, we performed immunofluorescent staining on the sections containing the MRR (Fig. 4). This type of investigation inherently leads to an underestimation of the number of the double-projecting cells, for several reasons: (i) we could not completely label the target brain areas without jeopardizing tracer leakage to adjacent brain areas, which we managed to avoid; (ii) MRR fibers may arborize only in a subregion of the target nucleus and these subregions may or may not be labeled by the tracer and (iii) MRR fibers may take up the injected tracer with low probability, if their arborization is scarce in the injection labeled area. Taken these limitations and the percentage of the injection labeled areas into account, we found a large amount of cells projecting to both injection labeled forebrain areas. For details, see Table 3. In the mouse having the largest injection labeled area (13 % of the HIPP and 13 % of the mPFC), about 9–12 % of the cells projecting to one area also projected to the other area.

To determine the neurochemical identity of these cells, we performed vGluT3 and 5HT labeling in the MRR of one mouse. We found, that more than 90 % of the double-projecting cells contained vGluT3, and the majority of those also contain 5HT (Table 3).

Single cells of the MRR project to the MS and mPFC simultaneously

To investigate whether the same MRR cells can project to the MS as well as to the mPFC, we injected the retrograde tracers CTB into the MS, and FG into the mPFC of both hemispheres of four mice. Then, we performed immunofluorescent staining on the sections containing the MRR (Fig. 5). In the mouse having the largest injection labeled area (23 % of the MS and 17 % of the mPFC), about 11–16 % of the cells projecting to one area also projected to the other area. In two mice, we checked the vGluT3 and 5HT content of the cells projecting to both forebrain areas. We found that 67–93 % of them contain vGluT3 and about one-third of these cells were immunoreactive for 5HT as well (Table 4).

Discussion

Using several immunohistochemical approaches in the mouse, we found in this study that: (1) NMDA receptors are present in the postsynaptic active zones of the synapses established by the MRR in the HIPP, MS and mPFC. (2) The majority of the cells in the MRR projecting to the mPFC are glutamatergic, similar to those projecting to HIPP and MS. (3) Several cells of the MRR project to more than one forebrain areas and they are also mostly glutamatergic. These data show that the majority of the output of the MRR is glutamatergic and it can act through NMDA receptor-containing synapses, suggesting that the primary function of the MRR may be to excite key GABAergic cells in the forebrain, while serotonin may be an important modulator of this transmission.

Possible role of NMDA receptors in the synapses established by MRR in the forebrain

Previously, we found in the rat (Varga et al. 2009) that a functional serotonergic and glutamatergic cotransmission is present in synapses established by the MRR in the HIPP and about 75 % of the amplitude of photostimulation-evoked excitatory postsynaptic potentials was glutamatergic at these synapses. The receptor content of the synapses established by MRR was examined only in the same study (Varga et al. 2009), where we showed their AMPA receptor content in the HIPP. However, here, in the mouse, we show that not only these synapses, but also other MRR synapses in the forebrain contain NMDA receptors. These two types of receptors are the typical components of the classical excitatory synapses and explain the robust, fast excitation conveyed by glutamatergic afferents.

MRR innervates its target cells efficiently: a subpopulation of hippocampal interneurons can receive up to 40 boutons from the MRR to their somata and dendrites (Freund et al. 1990; Aznar et al. 2004). Similar innervation of MRR fibers was found around parvalbumin- and calbindin-positive somata in the MS of the rat, establishing about 3–5 terminals per somata (Leranth and Vertes 1999; Aznar et al. 2004). We also observed this perisomatic innervation profile of the MRR in the mouse not only in the MS, but also in the mPFC and these large terminals were similar to those described by Kosofsky and Molliver (1987).

We found that the majority of the cells projecting to all of these brain areas are glutamatergic. Our results showed that a large proportion of the synapses established by these terminals are positive for NMDA receptors in every examined brain area. The proportion of GluN2A-positive synapses of the MRR is high in the HIPP, where, according

to our measurements, nearly 90 % of synapses established by the vGluT3-positive terminals of the MRR contain NMDA receptors. Furthermore, our calculation, based on our semi-quantitative data, showed similar amount of NMDA receptors in the synapses of MRR compared to that in local adjacent asymmetric synapses. These excitatory basket-like innervations can be highly effective in modulating or even overwriting the activity of the innervated cells. Indeed, we previously showed in the rat a disynaptic inhibition of hippocampal pyramidal cells by these interneurons after MRR stimulation (Varga et al. 2009). The similar anatomical composition of these synapses in the mouse HIPP, MS and mPFC suggests that MRR can exert a fast subcortical control not only in the HIPP but also in the other forebrain areas.

Interaction of synaptic NMDA receptors and the serotonergic neurotransmission

Interestingly, cooperation between the serotonergic and glutamatergic neurotransmitter system has already been described in different species in many central nervous system areas (Amilhon et al. 2010; de Bartolomeis et al. 2013) and NMDA receptors were also shown to take part in these regulatory mechanisms (Maura et al. 2000; MacLean and Schmidt 2001; Yuen et al. 2005). Functional $5HT_3$ receptors are present in the interneurons of the HIPP (Ropert and Guy 1991; McMahon and Kauer 1997; Varga et al. 2009), and they were also shown to be present in GABAergic cells of the MS and mPFC (Morales and Bloom 1997; Puig et al. 2004). Although, it was not possible to directly examine the possible synaptic co-localization of NMDA receptors and $5HT_3$ receptors, previously, we showed that MRR synapses in the rat HIPP act trough $5HT_3$ receptors and glutamate receptors (Varga et al. 2009). Here, we show that these glutamate receptors are at least partly NMDA receptors, which suggest their interaction in this connection as well. Interestingly, the current– voltage curve of the $5HT_3$ receptor is dependent on the extracellular Ca^{2+} level (McMahon and Kauer 1997), which may be temporarily depleted by NMDA receptors (Arens et al. 1992; Vassilev et al. 1997). In addition, depolarization mediated by $5HT_3$ receptor could also help to remove the voltage-dependent Mg^{2+} block from the NMDA receptors. However, $5HT_3$-like receptors were also shown to directly inhibit NMDA receptor-dependent responses in pyramidal cells of the mPFC in a longer timescale (Liang et al. 1998). In addition, 5HT was shown to directly block NMDA responses in rat ventral spinal cord cultures (Chesnoy-Marchais and Barthe 1996). Thus, upon strong MRR activation, serotonin could exert a direct temporary negative feedback of excitation, if these synapses became over-activated, protecting the cell from excitotoxicity. Taken together, the presence of NMDA receptors at these synapses can reveal new explanations to where these interactions may actually take place.

MRR as an ascending glutamatergic nucleus: the anatomical framework for synchronous excitation of key forebrain inhibitory neurons

The first studies in the literature that suggested an ascending non-serotonergic output from the rat MRR were based on retrograde labeling experiments, showing that 5HT-negative MRR cells project to the HIPP or MS (Köhler et al. 1982; Köhler and Steinbusch 1982; Acsády et al. 1996). Then, Aznar et al. (2004) found that only about one-third of the anterogradely traced fibers of the MRR are 5HT-positive in the HIPP CA1 and CA3, and hardly any of them are 5HT-positive in the MS and the diagonal band of Broca in the rat.

After that, Somogyi et al. (2004) showed that some vGluT3-positive terminals in the HIPP are also serotonergic. Then, Jackson et al. (2009) showed that projecting cells, retrogradely labeled from the HIPP or MS of the rat, may actually contain the vGluT3 in the MRR. Finally, we showed in the rat that these vGluT3-containing fibers can excite local interneurons in the HIPP (Varga et al. 2009).

In mouse, so far only one study examined the possible vGluT3 content of the MRR fibers. Amilhon et al. (2010) found that about half of the 5HT-positive fibers in the prelimbic cortex and HIPP of the mouse contain vGluT3. However, the possible presence of non-serotonergic projecting cells was not examined there. Here, our results show that the majority of cells in the MRR projecting to the HIPP, MS and mPFC contain vGluT3 with or without 5HT in the mouse (Table 2), suggesting that the glutamatergic MRR projection is fundamental.

Only a few studies examined whether single MRR cells in the rat can project to more forebrain areas simultaneously, but none of them examined the possible vGluT3 content of these double-projecting cells. Köhler and colleagues identified cells in the rat MRR, projecting either to the entorhinal cortex and HIPP or to the entorhinal cortex and MS simultaneously (Köhler et al. 1982; Köhler and Steinbusch 1982). In addition, it has been described that single serotonergic MRR cells of the rat can project to the MS and HIPP simultaneously (Acsády et al. 1996; McKenna and Vertes 2001). None of these studies described double-projecting non-serotonergic cells. Here, we described that there is a significant population of cells in the MRR that project to the HIPP and mPFC or the MS and mPFC simultaneously, and most of them are glutamatergic. This suggests that these cells can synchronously modulate different brain areas in a fast and precise manner through the excitation of the targeted inhibitory neurons. The HIPP, MS and mPFC are heavily interconnected through several direct and indirect pathways (Freund and Antal 1988; Semba 2000; Heidbreder and Groenewegen 2003; Takács et al. 2008), therefore, the activation of key GABAergic cells via excitatory inputs to these brain areas would be highly effective in the modulation of their synchronous activity patterns and cooperation.

Conclusion

Taken together, our findings further support that the MRR can exert a fast and effective control of inhibition in multiple forebrain areas through glutamatergic transmission. This effect can be mediated by NMDA receptors that can cooperate well with the serotonergic system. Moreover, we conclude that the majority of the MRR cells projecting to the HIPP, MS and mPFC are glutamatergic, and these cells are in a perfect position to orchestrate the network activity in these brain areas. Our findings shed light on the structural background of the powerful modulation exerted by a key subcortical modulatory center.

Acknowledgments

References

Acsády L, Halasy K, Freund TF. Calretinin is present in non-pyramidal cells of the rat hippocampus–III. Their inputs from the medianraphe and medialseptal nuclei. Neuroscience. 1993; 52(4):829–841. [PubMed: 7680801]

Acsády L, Arabadzisz D, Katona I, Freund TF. Topographic distribution of dorsal and median raphe neurons with hippocampal, septal and dual projection. Acta Biol Hung. 1996; 47(1–4):9–19. [PubMed: 9124016]

Amilhon B, Lepicard E, Renoir T, Mongeau R, Popa D, Poirel O, Miot S, Gras C, Gardier AM, Gallego J, Hamon M, Lanfumey L, Gasnier B, Giros B, El Mestikawy S. vGluT3 (vesicular glutamate transporter type 3) contribution to the regulation of serotonergic transmission and anxiety. J Neurosci. 2010; 30(6):2198–2210.10.1523/JNEUROSCI.5196-09.2010 [PubMed: 20147547]

Arens J, Stabel J, Heinemann U. Pharmacological properties of excitatory amino acid induced changes in extracellular calcium concentration in rat hippocampal slices. Can J Physiol Pharmacol. 1992; 70(Suppl):S194–S205. [PubMed: 1295671]

Assaf SY, Miller JJ. The role of a raphe serotonin system in the control of septal unit activity and hippocampal desynchronization. Neuroscience. 1978; 3(6):539–550. [PubMed: 151244]

Azmitia EC, Segal M. An autoradiographic analysis of the differential ascending projections of the dorsal and median raphe nuclei in the rat. J Comp Neurol. 1978; 179(3):641–667.10.1002/cne.901790311 [PubMed: 565370]

Aznar S, Qian ZX, Knudsen GM. Non-serotonergic dorsal and median raphe projection onto parvalbumin- and calbindin-containing neurons in hippocampus and septum. Neuroscience. 2004; 124(3):573–581.10.1016/j.neuroscience.2003.12.020 [PubMed: 14980728]

Bang SJ, Jensen P, Dymecki SM, Commons KG. Projections and interconnections of genetically defined serotonin neurons in mice. Eur J Neurosci. 2012; 35(1):85–96. doi:10.1111/j.1460-9568.2011.07936.x. [PubMed: 22151329]

Chesnoy-Marchais D, Barthe JY. Voltage-dependent block of NMDA responses by 5-HT agonists in ventral spinal cord neurones. Br J Pharmacol. 1996; 117(1):133–141. [PubMed: 8825354]

de Bartolomeis A, Buonaguro EF, Iasevoli F. Serotonin-glutamate and serotonin-dopamine reciprocal interactions as putative molecular targets for novel antipsychotic treatments: from receptor heterodimers to postsynaptic scaffolding and effector proteins. Psychopharmacology. 2013; 225(1):1–19. doi:10. 1007/s00213-012-2921-8. [PubMed: 23179966]

Dederen PJ, Gribnau AA, Curfs MH. Retrograde neuronal tracing with cholera toxin B subunit: comparison of three different visualization methods. Histochem J. 1994; 26(11):856–862. [PubMed: 7868356]

Dingledine R, Borges K, Bowie D, Traynelis SF. The glutamate receptor ion channels. Pharmacol Rev. 1999; 51(1):7–61. [PubMed: 10049997]

Freund TF, Antal M. GABA-containing neurons in the septum control inhibitory interneurons in the hippocampus. Nature. 1988; 336(6195):170–173.10.1038/336170a0 [PubMed: 3185735]

Freund TF, Gulyás AI, Acsády L, Görcs T, Tóth K. Serotonergic control of the hippocampus via local inhibitory interneurons. Proc Natl Acad Sci USA. 1990; 87(21):8501–8505. [PubMed: 1700433]

Fukaya M, Kato A, Lovett C, Tonegawa S, Watanabe M. Retention of NMDA receptor NR2 subunits in the lumen of endoplasmic reticulum in targeted NR1 knockout mice. Proc Natl Acad Sci USA. 2003; 100(8):4855–4860. doi:10.1073/pnas. 0830996100. [PubMed: 12676993]

Hamorsky KT, Kouokam JC, Bennett LJ, Baldauf KJ, Kajiura H, Fujiyama K, Matoba N. Rapid and scalable plant-based production of a cholera toxin B subunit variant to aid in mass vaccination against cholera outbreaks. PLoS Negl Trop Dis. 2013; 7(3):e2046. [PubMed: 23505583]

Heidbreder CA, Groenewegen HJ. The medial prefrontal cortex in the rat: evidence for a dorso-ventral distinction based upon functional and anatomical characteristics. Neurosci Biobe-hav Rev. 2003; 27(6):555–579.

Hensler JG. Serotonergic modulation of the limbic system. Neurosci Biobehav Rev. 2006; 30(2):203–214.10.1016/j.neubiorev.2005.06.007 [PubMed: 16157378]

Jackson J, Dickson CT, Bland BH. Median raphe stimulation disrupts hippocampal theta via rapid inhibition and state-dependent phase reset of theta-related neural circuitry. J Neuro-physiol. 2008; 99(6):3009–3026.10.1152/jn.00065.2008

Jackson J, Bland BH, Antle MC. Nonserotonergic projection neurons in the midbrain raphe nuclei contain the vesicular glutamate transporter vGluT3. Synapse. 2009; 63(1):31–41. doi:10. 1002/syn.20581. [PubMed: 18925658]

Klausberger T. GABAergic interneurons targeting dendrites of pyramidal cells in the CA1 area of the hippocampus. Eur J Neurosci. 2009; 30(6):947–957.10.1111/j.1460-9568.2009.06913.x [PubMed: 19735288]

Köhler C, Steinbusch H. Identification of serotonin and non-serotonin-containing neurons of the mid-brain raphe projecting to the entorhinal area and the hippocampal formation. A combined immunohistochemical and fluorescent retrograde tracing study in the rat brain. Neuroscience. 1982; 7(4):951–975. [PubMed: 7048127]

Köhler C, Chan-Palay V, Steinbusch H. The distribution and origin of serotonin-containing fibers in the septal area: a combined immunohistochemical and fluorescent retrograde tracing study in the rat. J Comp Neurol. 1982; 209(1):91–111. doi:10. 1002/cne.902090109. [PubMed: 6749914]

Kosofsky BE, Molliver ME. The serotoninergic innervation of cerebral cortex: different classes of axon terminals arise from dorsal to median raphe nuclei. Synapse. 1987; 1(2):153–168. doi:10. 1002/syn.890010204. [PubMed: 2463687]

Lanciego JL, Wouterlood FG. A half century of experimental neuroanatomical tracing. J Chem Neuroanat. 2011; 42(3):157–183.10.1016/j.jchemneu.2011.07.001 [PubMed: 21782932]

Leranth C, Vertes RP. Median raphe serotonergic innervation of medial septum/diagonal band of broca (MSDB) parvalbumin-containing neurons: possible involvement of the MSDB in the desynchronization of the hippocampal EEG. J Comp Neurol. 1999; 410(4):586–598. doi:10.1002/(SICI)1096-9861(19990809)410: 4<586:AID-CNE6>3.0.CO;2-H. [PubMed: 10398050]

Liang X, Arvanov VL, Wang RY. Inhibition of NMDA-receptor mediated response in the rat medial prefrontal cortical pyramidal cells by the 5-HT3 receptor agonist SR 57227A and 5-HT: intracellular studies. Synapse. 1998; 29(3):257–268.10.1002/(SICI)1098-2396(199807)29:3<257:AID-SYN8>3.0.CO;2-5 [PubMed: 9635896]

MacLean JN, Schmidt BJ. Voltage-sensitivity of motoneuron NMDA receptor channels is modulated by serotonin in the neonatal rat spinal cord. J Neurophysiol. 2001; 86(3):1131–1138. [PubMed: 11535663]

Malenka RC, Bear MF. LTP and LTD: an embarrassment of riches. Neuron. 2004; 44(1):5–21.10.1016/j.neuron.2004.09.012 [PubMed: 15450156]

Maura G, Marcoli M, Pepicelli O, Rosu C, Viola C, Raiteri M. Serotonin inhibition of the NMDA receptor/nitric oxide/cyclic GMP pathway in human neocortex slices: involvement of 5-HT(2C) and 5-HT(1A) receptors. Br J Pharmacol. 2000; 130(8):1853–1858.10.1038/sj.bjp.0703510 [PubMed: 10952674]

McKenna JT, Vertes RP. Collateral projections from the median raphe nucleus to the medial septum and hippocampus. Brain Res Bull. 2001; 54(6):619–630. [PubMed: 11403988]

McMahon LL, Kauer JA. Hippocampal interneurons are excited via serotonin-gated ion channels. J Neurophysiol. 1997; 78(5):2493–2502. [PubMed: 9356400]

Morales M, Bloom FE. The 5-HT3 receptor is present in different subpopulations of GABAergic neurons in the rat telencephalon. J Neurosci. 1997; 17(9):3157–3167. [PubMed: 9096150]

Papp EC, Hajos N, Acsády L, Freund TF. Medial septal and median raphe innervation of vasoactive intestinal polypeptide-containing interneurons in the hippocampus. Neuroscience. 1999; 90(2):369–382. [PubMed: 10215142]

Paxinos, G.; Franklin, KBJ. The mouse brain in stereotaxic coordinates. 4th. Academic Press; Waltham: 2012.

Puig MV, Santana N, Celada P, Mengod G, Artigas F. In vivo excitation of GABA interneurons in the medial prefrontal cortex through 5-HT3 receptors. Cereb Cortex. 2004; 14(12):1365–1375.10.1093/cercor/bhh097 [PubMed: 15166106]

Ropert N, Guy N. Serotonin facilitates GABAergic transmission in the CA1 region of rat hippocampus in vitro. J Physiol. 1991; 441:121–136. [PubMed: 1687746]

San Paulo A, García R. High-resolution imaging of antibodies by tapping-mode atomic force microscopy: attractive and repulsive tip-sample interaction regimes. Biophys J. 2000; 78(3):1599–1605.10.1016/S0006-3495(00)76712-9 [PubMed: 10692344]

Semba K. Multiple output pathways of the basal forebrain: organization, chemical heterogeneity, and roles in vigilance. Behav Brain Res. 2000; 115(2):117–141. [PubMed: 11000416]

Somogyi J, Baude A, Omori Y, Shimizu H, El Mestikawy S, Fukaya M, Shigemoto R, Watanabe M, Somogyi P. GABAergic basket cells expressing cholecystokinin contain vesicular glutamate transporter type 3 (vGluT3) in their synaptic terminals in hippocampus and isocortex of the rat. Eur J Neurosci. 2004; 19(3):552–569. [PubMed: 14984406]

Szabadits E, Cserép C, Szonyi A, Fukazawa Y, Shigemoto R, Watanabe M, Itohara S, Freund TF, Nyiri G. NMDA receptors in hippocampal GABAergic synapses and their role in nitric oxide signaling. J Neurosci. 2011; 31(16):5893–5904.10.1523/JNEUROSCI.5938-10.2011 [PubMed: 21508214]

Takács VT, Freund TF, Gulyás AI. Types and synaptic connections of hippocampal inhibitory neurons reciprocally connected with the medial septum. Eur J Neurosci. 2008; 28(1):148–164.10.1111/j.1460-9568.2008.06319.x [PubMed: 18662340]

Takács VT, Freund TF, Nyiri G. Neuroligin 2 is expressed in synapses established by cholinergic cells in the mouse brain. PLoS One. 2013; 8(9):e72450.10.1371/journal.pone.0072450 [PubMed: 24039767]

Varga C, Sík A, Lavallée P, Deschênes M. Dendroarchitecture of relay cells in thalamic barreloids: a substrate for cross-whisker modulation. J Neurosci. 2002; 22(14):6186–6194. [PubMed: 12122077]

Varga V, Losonczy A, Zemelman BV, Borhegyi Z, Nyiri G, Domonkos A, Hangya B, Holderith N, Magee JC, Freund TF. Fast synaptic subcortical control of hippocampal circuits. Science. 2009; 326(5951):449–453.10.1126/science.1178307 [PubMed: 19833972]

Varoqueaux F, Jamain S, Brose N. Neuroligin 2 is exclusively localized to inhibitory synapses. Eur J Cell Biol. 2004; 83(9):449–456.10.1078/0171-9335-00410 [PubMed: 15540461]

Vassilev PM, Mitchel J, Vassilev M, Kanazirska M, Brown EM. Assessment of frequency-dependent alterations in the level of extracellular Ca2+ in the synaptic cleft. Biophys J. 1997; 72(5):2103–2116.10.1016/S0006-3495(97)78853-2 [PubMed: 9129812]

Vertes RP, Kocsis B. Brainstem-diencephalo-septohippocam-pal systems controlling the theta rhythm of the hippocampus. Neuroscience. 1997; 81(4):893–926. [PubMed: 9330355]

Vertes RP, Martin GF. Autoradiographic analysis of ascending projections from the pontine and mesencephalic reticular formation and the median raphe nucleus in the rat. J Comp Neurol. 1988; 275(4):511–541.10.1002/cne.902750404 [PubMed: 3192756]

Vertes RP, Fortin WJ, Crane AM. Projections of the median raphe nucleus in the rat. J Comp Neurol. 1999; 407(4):555–582. doi:10. 1002/(SICI)1096-9861(19990517)407:4<555:AID-CNE7>3.0. CO; 2-E. [PubMed: 10235645]

Watanabe M, Fukaya M, Sakimura K, Manabe T, Mishina M, Inoue Y. Selective scarcity of NMDA receptor channel subunits in the stratum lucidum (mossy fibre-recipient layer) of the mouse hippocampal CA3 subfield. Eur J Neurosci. 1998; 10(2):478–487. [PubMed: 9749710]

Yuen EY, Jiang Q, Chen P, Gu Z, Feng J, Yan Z. Serotonin 5-HT1A receptors regulate NMDA receptor channels through a microtubule-dependent mechanism. J Neurosci. 2005; 25(23):5488–5501.10.1523/JNEUROSCI.1187-05.2005 [PubMed: 15944377]

Zhang L, Ren G. IPET and FETR: experimental approach for studying molecular structure dynamics by cryo-electron tomography of a single-molecule structure. PLoS One. 2012; 7(1):e30249.10.1371/journal.pone.0030249 [PubMed: 22291925]
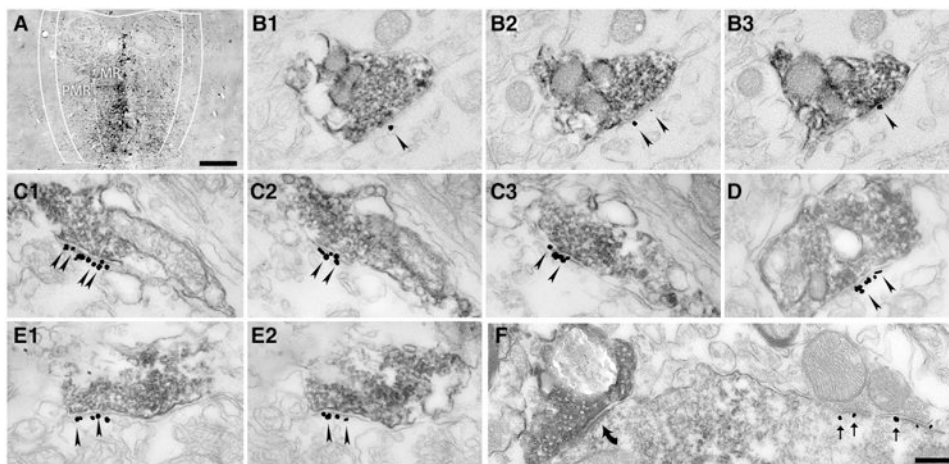
Fig. 1.
NMDA receptors are present in the postsynaptic active zones of MRR-HIPP. Synapses a
Light micrograph showing a representative injection site of 10 kDa BDA into the median
raphe region that comprises of the median raphe (MR) and paramedian raphe (PMR). *Scale
bar* 200 μm. **b–f** Electron micrographs of synapses show combined immunogold–
immunoperoxidase reactions from the border of str. radiatum and lacunosum-moleculare of
the CA1 region of the HIPP. *Scale bar* for all: 300 nm. b_1–b_3, c_1–c_3, **d**, e_1–e_2 The
immunogold particles (*arrowheads*) label the GluN2A subunit of the NMDA receptor
located postsynaptically in the synapses established by presynaptic terminals of MRR fibers,
filled with dark DAB precipitate, corresponding either to the anterograde tracer BDA (b_1–
b_3) or to vGluT3 (**c–e**) labeling. b_1–b_3, c_1–c_3 and e_1–e_2 Consecutive sections of the very
same synapses, respectively. **f** Neuroligin-2 (immunogold particles, *thin arrows*) is present
on the postsynaptic side of a putative GABAergic synapse established by a vGluT3-negative
terminal, but it is absent from the synapse of a vGluT3-positive terminal (*thick black arrow*)
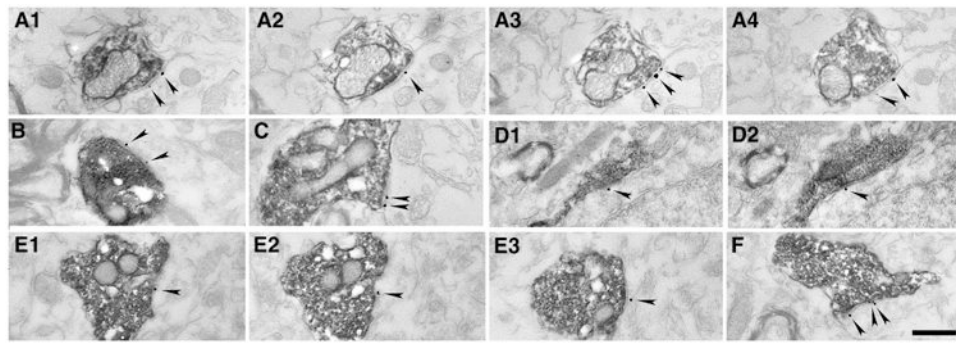
Fig. 2.

NMDA receptors are present in the postsynaptic active zones of synapses established by MRR in the MS and mPFC. Electron micrographs of synapses show combined immunogold–immunoperoxidase reactions from the MS (**a_1–a_4, b, c**) and mPFC (**d_1–d_2, e_1–e_3, f**). The immunogold particles (*arrowheads*) show the GluN2A subunit of the NMDA receptor postsynaptically in the synapses established by presynaptic terminals of MRR fibers, labelled with the anterograde tracer BDA (dark DAB precipitate). **a_1–a_4, d_1–d_2** and **e_1–e_3** Show the consecutive sections of the very same synapses, respectively. *Scale bar* 500 nm
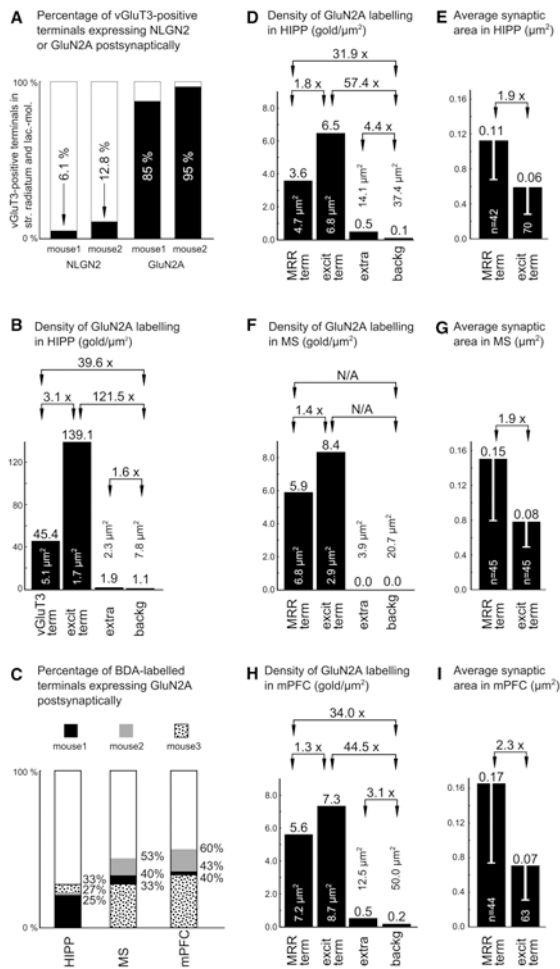
Fig. 3.

Graphs summarizing the data acquired with immunoelectron microscopy. **a** The columns show vGluT3-positive terminals that establish synapses on somata or proximal dendrites of interneurons at the distal dendritic region of the CA1. The percentages show the proportions of synapses containing NLGN2 or GluN2A postsynaptically, respectively. **b** Average densities of the immunogold particles in different membrane domains of the two mice used for vGluT3– GluN2A double immunohistochemical measurements. The columns show the density of immunogold particles in synapses established by vGluT3-positive (mostly MRR) terminals (vGluT3 term) or local excitatory terminals (excit term) and extrasynaptic labeling measured 200 nm away from both edges of the postsynaptic side of the excitatory synapses (extra), and background labeling measured on the presynaptic side of the same synapses (backg). The total amount of measured membrane domain area is indicated in μm^2 s, respectively. **c** Percentages of the synapses established by BDA-labelled terminals containing postsynaptic GluN2A labeling in the HIPP, MS and mPFC. The data were collected from three mice. **d, f, h** Average densities of the immunogold particles in different membrane domains in three mice used for BDA-GluN2A double immunohistochemical measurements in the HIPP, MS and mPFC, respectively. The columns show the density of immunogold particles in synapses established by BDA-labelled MRR inputs (MRR term) or

local excitatory terminals (excit term) and extrasynaptic labeling measured on a 200-nm-long extrasynaptic membrane segment from both edges of the very same synapses (extra), and background labeling measured on the presynaptic side of the same synapses (backg). The total amount of measured membrane domain area is indicated in μm^2 s. **e, g, i** The columns show the average synaptic areas of raphe inputs (MRR term) and local excitatory synapses (excit term) in three mice used in BDA-GluN2A double immunohistochemical measurements in the HIPP, MS and mPFC, respectively. Error bars indicate standard deviations. The total number of totally reconstructed synapses are indicated in the columns
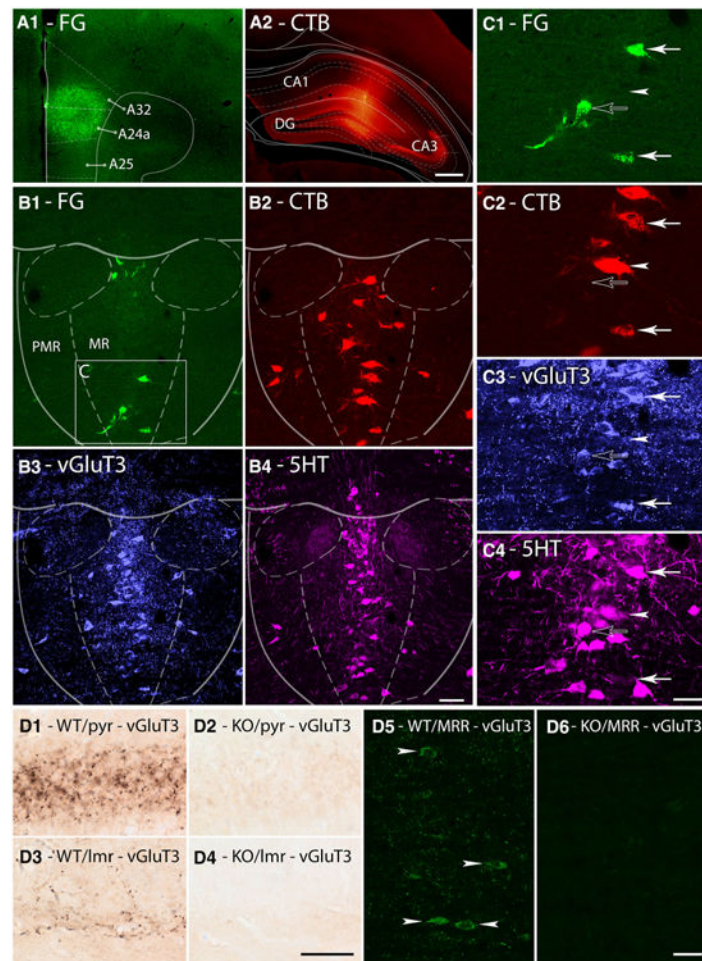
Fig. 4.

Single cells of the median raphe project to the HIPP and mPFC simultaneously. a_1–a_2 Fluorescent micrographs show representative injection sites of FG (a_1) and CTB (a_2) into the ipsilateral mPFC and HIPP, respectively. A24a, A25, and A32 subregions of the mPFC, the CA1, CA3 regions of the HIPP and the dentate gyrus (DG) are indicated in the images. *Scale bar* 200 μm. b_1–b_4 Maximal intensity projections of three image planes of confocal laser scanning images show the same representative median raphe region comprising of median raphe (MR) and paramedian raphe (PMR). FG (*green*) labels cells projecting to the mPFC, CTB (*red*) labels cells projecting to the HIPP, vGluT3 (*blue*) labels glutamatergic cells and 5HT (*magenta*) labels serotonergic cells. The area **c** on B1 indicates the position of images (c_1–c_4). *Scale bar* 100 μm. c_1–c_4 Magnified images of the same cluster of MRR cells. *Open arrow* marks a cell projecting to the mPFC, containing vGluT3 and 5HT; *arrowhead* marks a cell projecting to the HIPP, immunoreactive only for 5HT; *closed arrows* mark cells that project to both forebrain areas; the upper cell contains vGluT3 and 5HT, while the lower cell contains only vGluT3. *Scale bar* 30 μm. d_1–d_6 Images showing the specificity of vGluT3-staining using the guinea pig anti-vGluT3 antibody on wild-type (WT) and on vGluT3−/− null-mutant (KO) mice. Representative images show immunoperoxidase reactions in the pyramidal cell layer (pyr, d_1–d_2) and in the border of

stratum radiatum and lacunosum-moleculare (lmr, **d$_3$**–**d$_4$**) of the HIPP. Maximal intensity projections of three image planes of confocal laser scanning images show immunofluorescent reactions in the MRR (**d$_5$**–**d$_6$**). *Arrowheads* show vGluT3-positive somata in the WT mouse, while no specificlike staining was observed in the KO mouse. *Scale bars* 30 μm
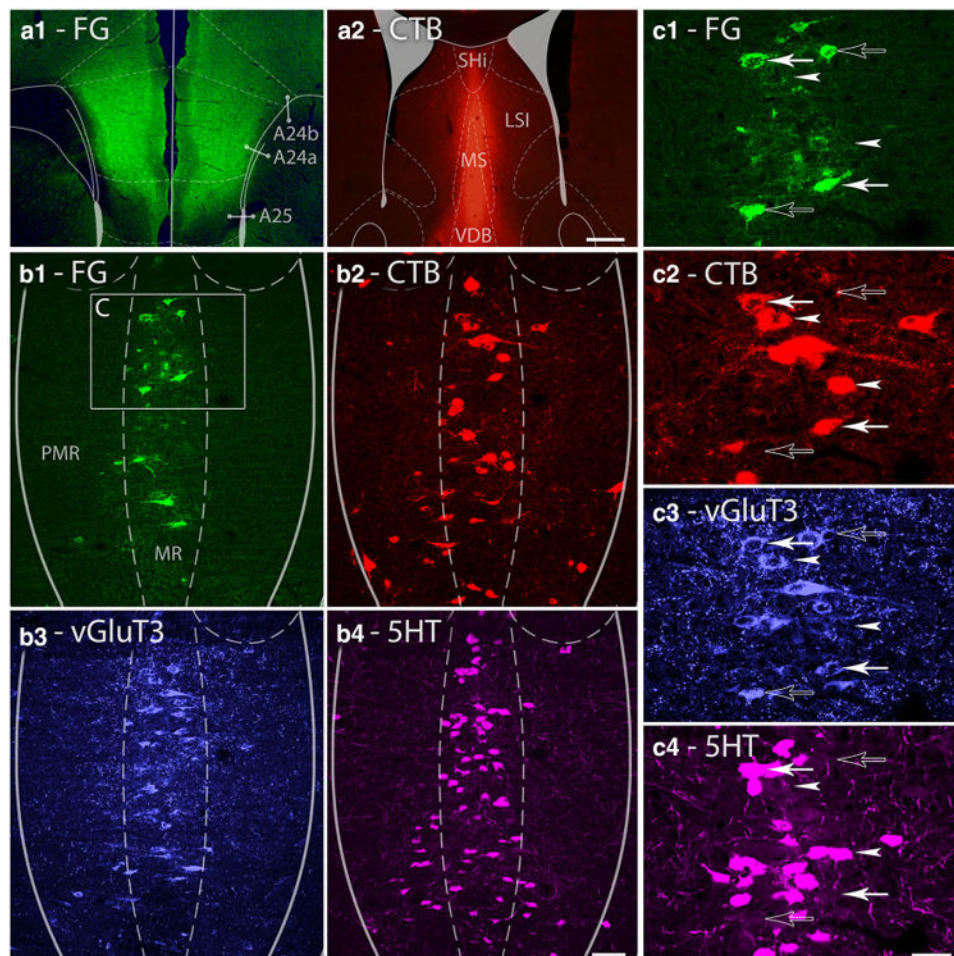
Fig. 5.

Single cells of the median raphe project to the MS and mPFC simultaneously. **a1**–**a2** Fluorescent micrographs show representative injection sites of FG (**a1**) and CTB (**a2**) into the bilateral mPFC and MS, respectively. A24a, A24b, and A25 subregions of the mPFC, medial septum (MS), vertical limb of the diagonal band of Broca (VDB), septohippocampal nucleus (SHi) and lateral septum, intermediate part (LSI) are indicated on the images. *Scale bar* 200 μm. **b1**–**b4** Maximal intensity projection images of three image planes of confocal laser scanning micrographs show the same representative median raphe region comprising of median raphe (MR) and paramedian raphe (PMR). FG (*green*) labels cells projecting to the mPFC, CTB (*red*) labels cells projecting to the MS, vGluT3 (*blue*) labels glutamatergic cells and 5HT (*magenta*) labels serotonergic cells. The area **c** on **b1** indicates the position of images **c1**–**c4**. *Scale bar* 100 μm. **c1**–**c4** Magnified images of the same cluster of median raphe cells. *Open arrows* mark cells projecting to the mPFC, containing only vGluT3; *arrowheads* mark cells projecting to the MS; the upper cell contains only vGluT3, while the lower cell contains only 5HT; *closed arrows* mark cells that project to both forebrain areas; the upper cell contains vGluT3 and 5HT, while the lower cell contains only vGluT3. *Scale bar* 30 μm

Table 1

Antibody specifications

Raised against	Raised in	Protein cc. of stock solution	Dilution	Source	Catalog number	Lot number	Characterized
Neuroligin 2	Rabbit	1,000 μg/ml	1:600	Synaptic Systems	129 203	10	Takács et al. (2013)
GluN2A	Rabbit	542 μg/ml	1:150–1:250	Gift of M. Watanabe	–	–	Watanabe et al. (1998)
vGluT3	Guinea pig	Not available	1:1,000–1:4,000	Millipore	AB 5421	LV1453193	Szabadits et al. (2011), present study
serotonin	Rat	Not available	1:500	Millipore	MAB 352	2168248	Amilhon et al. (2010)
Fluoro-Gold	Rabbit	Not available	1:10,000–1:30,000	Millipore	AB153	2003657	Varga et al. (2002)
Cholera toxin B subunit	Goat	Not available	1:20,000	List Biologicals	703	7032A7	Dederen et al. (1994)
Cholera toxin B subunit	Mouse	1,000 μg/ml	1:400	Abcam	ab1003	–	Hamorsky et al. (2013)

Conjugated with	Raised in	Raised against	Dilution	Source	Catalog number		Characterized
1.4 nm nanogold	Goat	Rabbit	1:100–1:300	Nanoprobes	#2004		Fab'-fragment
Biotin	Goat	Guinea pig	1:200	Vector laboratories	BA-7000		Whole IgG
Alexa 647	Chicken	Rat	1:500	Life technologies	A-21472		Whole IgG
Alexa 488	Goat	Guinea pig	1:1,000	Molecular probes	A-11073		Whole IgG
Alexa 488	Donkey	Rabbit	1:500–1:1,000	Life technologies	A-21206		Whole IgG
Alexa 594	Donkey	Goat	1:500	Life technologies	A-11058		Whole IgG
DyLight 549	Donkey	Mouse	1:500	Jackson immunoresearch	715-505-151		Whole IgG
DyLight 405	Streptavidin	Not antibody	1:500	Jackson immunoresearch	016-470-084		Streptavidin

Table 2

Neurochemical properties of retrogradely labeled cells projecting to different forebrain areas

Injected target area	Number of retrogradely labeled cells in MRR	Neurochemical identity of retrogradely labeled cells in MRR			
		vGluT3+ and 5HT+ (%)	Only vGluT3+ (%)	Only 5HT+ (%)	Unlabeled (%)
Hippocampus (mouse 5)	391	49	31	8	12
Medial septum (mouse 6)	850	19	34	13	34
Medial septum (mouse 7)	710	21	47	10	21
Medial prefrontal cortex (mouse 5)	506	32	38	21	9
Medial prefrontal cortex (mouse 6)	555	24	45	16	15
Medial prefrontal cortex (mouse 7)	334	29	46	10	15

Table 3

Hippocampus-mPFC double retrograde tracing experiments and neurochemical properties of double-projecting cells of the MRR

Animal ID number	Mouse 1	Mouse 2	Mouse 5
Percentage show the volume of the hippocampus that was labeled with the injected tracer (%)	11	12	13
Percentage show the volume of the unilateral mPFC that was labeled with the injected tracer (%)	8	9	13
Percentage of the cells projecting to the injection labeled mPFC area out of all cells backlabeled from the hippocampus	9/166 (5.4 %)	11/96 (11.5 %)	46/391 (11.9 %)
Percentage of the cells projecting to the injection labeled HIPP area out of all cells backlabeled from the mPFC	9/156 (5.8 %)	11/304 (3.6 %)	46/506 (8.7 %)
Neurochemical identity of cells that project to both flooded forebrain areas			
vGluT3+ and 5HT+	–	–	71 %
Only vGluT3+	–	–	20 %
Only 5HT+	–	–	9%
Unlabeled	–	–	0%

Table 4

MS-mPFC double retrograde tracing experiments and neurochemical properties of double-projecting cells of the MRR

Animal ID number	Mouse 3	Mouse 4	Mouse 6	Mouse 7
Percentage show the volume of the MS that was labeled with the injected tracer (%)	16	11	23	9
Percentage show the volume of the bilateral mPFC that was labeled with the injected tracer (%)	21	24	17	21
Percentage of the cells projecting to the injection labeled mPFC area out of all cells backlabeled from the MS	23/395 (5.8 %)	30/319 (9.4 %)	91/850 (10.9 %)	64/710 (9.2 %)
Percentage of the cells projecting to the injection labeled MS area out of all cells backlabeled from the mPFC	23/686 (3.4 %)	30/1,050 (2.9 %)	91/555(16.0 %)	64/334 (18.6 %)
Neurochemical identity of cells that project to both flooded forebrain areas				
vGluT3+ and 5HT+	–	–	32 %	37 %
Only vGluT3+	–	–	35 %	56 %
Only 5HT+	–	–	15 %	5%
Unlabeled	–	–	18 %	3%